Synthesis of Water-Soluble Iron−Gold Alloy Nanoparticles

Naween Dahal and Viktor Chikan*

Department of Chemistry, Kansas State University, Manhattan, Kansas 66506-3701

Jacek Jasinski[†] and Valerie J. Leppert

School of Engineering, University of California at Merced, Merced California 95344

In this study, a synthetic method to produce water-soluble iron−gold (Fe−Au) alloy nanoparticles is described. The diameter of the alloy nanoparticles is 4.9 ± 1.0 and 3.8 ± 1.0 nm for two different precursors of iron, ferrous sulfate heptahydrate (Fe^{2+}) and iron pentacarbonyl (Fe^0). The X-ray powder diffraction of the alloyed nanoparticles shows an appreciable shift in 2θ peak positions relative to pure gold or iron. Using Vegard's law, we estimated the particle's iron content to be 14.8 ± 4.7 mol %. The lattice constant of the alloy nanoparticles is found to be 4.0449 ± 0.0375 Å. The high-resolution transmission electron microscopy images show the presence of icosahedral structures in agreement with the previous high temperature synthesis of the Fe−Au alloy nanoparticles. The optical absorption of the alloy nanoparticles is distinctive from pure gold nanoparticles and shows a relatively narrow absorption band in the range of 642−662 nm depending upon the amount of gold precursor used.

Introduction

Bimetallic nanoparticles are promising to significantly extend the functionality of single component metallic catalysts. Bimetallic nanoparticles containing gold as one of the elements have begun to show opportunities for developing constituents of fuel cell catalysts.[1−4] Several research groups have already demonstrated diverse production techniques of bimetallic nanoparticles of this type. A large portion of the studies focus on Fe−Au core−shell nanoparticles.[5−11] The combination of either iron or iron oxide core and gold shell is specifically appealing because gold is a noble metal and provides an established platform for surface functionalization.[10,11] Additionally, the shell provides protection against oxidation and helps to maintain long-term stability of the particles.[5−11] Unfortunately, the core−shell particles have

their own challenges. First, the gold shell forms a poor diffusion barrier because of the high density of the grain boundaries at the gold surface.[12−14] Second, it is somewhat difficult to control the uniformity and thickness of the metal coating. On the other hand, with Fe−Au alloy nanoparticles, these effects may be minimized.

Fe−Au alloy nanoparticles are solid solutions where iron atoms substitute gold sites in the face center cubic lattice. At low iron content the gold-rich fcc solid solution is the predominant phase and exhibits magnetic spin glass properties.[15−17] Incorporation of even a little amount of iron increases the density of defective sites in the alloy nanoparticles and helps to increase the catalytic activity. In the literature, there are only a few reports concerning the preparation of Fe−Au alloy nanoparticles; pulsed laser deposition,[15] carbon film deposition at very high temperature (1600 K) in the presence of helium flow[12] and electrodeposition.[13] Very recently, Chiang et al. prepared Fe−Au alloy nanoparticles by reduction of gold acetate and thermal decomposition of iron pentacarbonyl at 300 °C.[14] At this point, a more robust synthesis is needed to better assist the broader exploitation of the Fe−Au nanoparticles.

In this paper, a relatively low temperature synthesis of Fe−Au alloy nanoparticles is presented using two different iron precursors. The size of the nanoparticles ranges between

* To whom all correspondence should be addressed. E-mail: chikan@ksu.edu.
† Current address: Institute for Advanced Materials and Renewable Energy, University of Louisville, Louisville, KY 40292.

(1) Haruta, M. *Catal. Today* **1997,** *36* (1), 153–166.
(2) Haruta, M.; Date, M. *Appl. Catal., A* **2001,** *222* (1−2), 427–437.
(3) Zhou, B. H. S.; Gabor, A. S. *Nanotechnology in Catalysis*; Kluwer Academic/Plenum publisher: New York, 2004; Vol. 1.
(4) Klabunde, K. J. *Nanoscale Materials in Chemistry*; John Wiley & Sons: New York, 2001.
(5) Cushing, B. L.; Kolesnichenko, V. L.; O'Connor, C. J. *Chem. Rev.* **2004,** *104* (9), 3893–3946.
(6) Zhou, W. L.; Carpenter, E. E.; Lin, J.; Kumbhar, A.; Sims, J.; O'Connor, C. J. *Eur. Phys. J. D* **2001,** *16* (1−3), 289–292.
(7) Ban, Z. H.; Barnakov, Y. A.; Golub, V. O.; O'Connor, C. J. *J. Mater. Chem.* **2005,** *15* (43), 4660–4662.
(8) Wang, L. Y.; Luo, J.; Maye, M. M.; Fan, Q.; Qiang, R. D.; Engelhard, M. H.; Wang, C. M.; Lin, Y. H.; Zhong, C. J. *J. Mater. Chem.* **2005,** *15* (18), 1821–1832.
(9) Carpenter, E. E.; Kumbhar, A.; Wiemann, J. A.; Srikanth, H.; Wiggins, J.; Zhou, W. L.; O'Connor, C. J. *Mater. Sci. Eng., A* **2000,** *286* (1), 81–86.
(10) Cho, S. J.; Idrobo, J. C.; Olamit, J.; Liu, K.; Browning, N. D.; Kauzlarich, S. M. *Chem. Mater.* **2005,** *17* (12), 3181–3186.
(11) Zhang, L. X.; Sun, X. P.; Song, Y. H.; Jiang, X.; Dong, S. J.; Wang, E. A. *Langmuir* **2006,** *22* (6), 2838–2843.

(12) Saha, D. K.; Koga, K.; Takeo, H. *Eur. Phys. J. D* **1999,** *9* (1−4), 539–542.
(13) Lu, D. L.; Domen, K.; Tanaka, K. *Langmuir* **2002,** *18* (8), 3226–3232.
(14) Chiang, I. C.; Chen, D. H. *Adv. Funct. Mater.* **2007,** *17* (8), 1311–1316.
(15) Chang, W. S.; Park, J. W.; Rawat, V.; Sands, T.; Lee, G. U. *Nanotechnology* **2006,** *17* (20), 5131–5135.
(16) Terzieff, P.; Gasser, J. G. *J. Phys.: Condens. Matter* **1994,** *6* (3), 603–612.
(17) Cannella, V.; Mydosh, J. A. *Phys. Rev. B* **1972,** *6* (11), 4220–&.

Table 1. Synthesis Condition, Particle Size, Composition, and Stability of Fe−Au Alloy Nanoparticles

sample prepared	precursors		temperature (°C)	ligand used	reducing agent	particle size (nm)	composition at 1:1 mol ratio
	iron	gold					
Fe−Au alloy	Fe(CO)$_5$	HAuCl$_4$·3H$_2$O	110	3-mercapto-1-propane Sulphonic acid	NaBH$_4$	3.8 ± 1.0	14.8 ± 4.7 mol % iron
Fe−Au alloy	FeSO$_4$·7H$_2$O	HAuCl$_4$·3H$_2$O	110	3-mercapto-1-propane Sulphonic acid	NaBH$_4$	4.9 ± 1.0	not calculated

4 to 6 nm. The iron content of the Fe−Au nanoparticles that is calculated form Vegards law is ~14.8 ± 4.7 mol % iron.[12,13,15] The UV−visible absorption spectra of Fe−Au alloy nanoparticles are different from pure iron or gold nanoparticles. Namely, if the plasmon resonance of the gold nanoparticle is considered as a reference, then the alloy nanoparticles show a significant red shift (approximately 100 nm).

Experimental Section

Fe−Au nanoparticles are produced via iron sulfate heptahydrate and iron pentacarbonyl. The description of the synthesis is described below. The synthesis condition, precursors used during the synthesis, their composition, size, and stability of the samples are presented in Table 1.

Preparation of Fe−Au Alloy Nanoparticles from Iron Sulfate Heptahydrate. In a typical synthesis, (0.08 mol) of (di-*n*-dodecyl) dimethylammonium bromide (99%) (DDAB) is dissolved in 20 mL of toluene (99%) in a three-necked flask under an argon atmosphere. The solution is stirred for 15 min at 110 °C; 0.02 mol of freshly prepared aqueous iron sulfate heptahydrate (99%) in 0.5 mL of double distilled water is then injected rapidly. The solution becomes turbid right away. After 2 min, 1.5 mL of sodium borohydride (98%) 2 M in aqueous solution is added. The solution turns to ash color with black colloids floating all around the solution. Twenty minutes later, a solution containing gold chloride is injected into the iron nanoparticle seed solution. The 1.5 mL gold chloride solution consists of 0.02 mol of gold(III) chloride trihydrate (99%) and 0.6 mol 3-mercapto-1-propansulphonicacid sodium salt (90%). When the color of the solution turns red, 1.5 mL of 2 M aqueous sodium borohydride is again added to reduce the gold chloride to gold. The color of the solution turns purple and slowly the purple color disappears. The final solution has a very faint reddish color. The solution is stirred for 30 min. Finally, 0.5 mL of 2 M aqueous sodium borohydride is added to the solution. The entire solution is heated at 84 °C for 3 h.

Preparation of Fe−Au Alloy Nanoparticles from Iron Pentacarbonyl. Alternatively, Fe−Au alloy nanoparticles are prepared under argon atmosphere via thermal decomposition of iron pentacarbonyl. In a typical synthesis, 0.002 mol of iron pentacarbonyl (99%) is injected at 110 °C into a three-necked flask containing 0.08 mol of DDAB and 20 mL of toluene. Initially, the color of the solution is yellow and it immediately turns a reddish color. A black solution is obtained after heating it for 20 min. Gold precursors and ligands are added as mentioned above. Two milliliters of aqueous sodium borohydride is added dropwise into the entire solution. Finally, a black greenish shining powder of iron−gold alloy nanoparticles is obtained.

Purification of the Samples. For purification, the crude mixture is mixed with ethanol (99%) and centrifuged for 15 min at 7000 rpm. In the first step, the precipitate is washed with ethanol and chloroform. This step is repeated several times. The dark greenish solid sample is collected and vaccum-dried for 10 h. The dried sample is placed in magnetic field for magnetic separation. Only the magnetic part is collected for further characterization. The

nanoparticles are easily dispersed in water. The approximate yield of the reactions is 30% by weight.

Results and Discussions

In this synthesis of Fe−Au alloy nanoparticles, the precursor molecules are injected into a hot solvent containing coordinating ligands. The addition of reducing agent, sodium borohydride is carried out in several steps, which leads to the formation of alloy nanoparticles. Figure 1a represents the low-resolution transmission electron microscope (TEM) image of Fe−Au alloys obtained from Fe^0 precursor, iron pentacarbonyl with an initial molar ratio of 1:1. Figure 1c shows the histogram of the corresponding particles obtained from Fe^0 precursor. The average size of the particles is calculated to be 3.8 ± 1.0 nm. Figure 1b represents the TEM image of Fe−Au alloy obtained from Fe^{2+} precursor revealing the inhomogeneous nucleation of iron on gold. The particle distribution shows some degree of polydispersity. The histogram of the Fe−Au nanoparticles from Fe^{2+} precursor is indicated in Figure 1d. The average size of these particles is found to be 4.9 ± 1.0 nm. Figure 1a inset shows the higher magnification image of the Fe−Au nanoparticles obtained form Fe^0 precursor. Within the resolution of the low resolution TEM, the image reveals irregularly shaped, multifaceted nanocrystals with sharp edges.

Figure 2 shows the UV−visible absorption spectra of Fe−Au alloy nanoparticles prepared using either Fe^{2+} or Fe^0 as an iron source. Both alloy nanoparticles show two
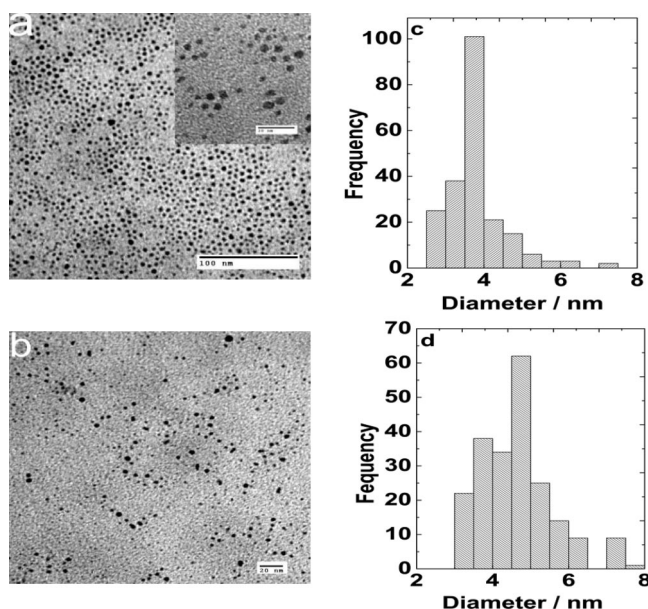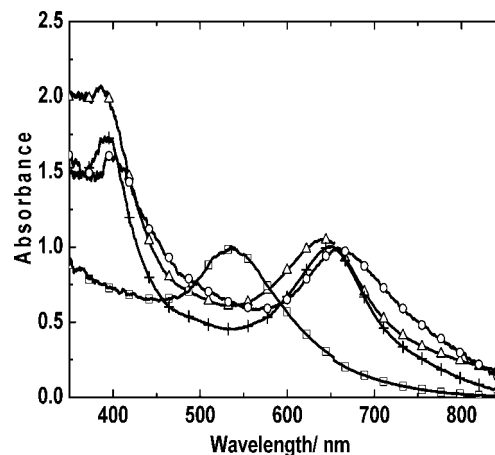

Figure 1. (a) TEM image of iron−gold alloy nanoparticles obtained from Fe^0 precursor. (b) TEM images of iron−gold alloy nanoparticles obtained from Fe^{2+} precursor. (c) Size histogram of alloy nanoparticles from Fe^0 precursor. (d) Size histogram of alloy nanoparticles from Fe^{2+} precursor.
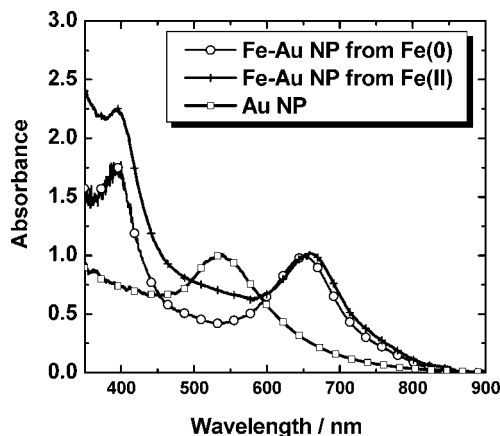
Figure 2. UV−visible absorption spectra (in water) of pure gold nanoparticles (open square) and gold iron alloy nanoparticles (NP) obtained from Fe^{2+} (plus) and Fe^0 precursor (circle).

Figure 3. UV−visible absorption spectra (in water) for pure gold and iron−gold alloy nanoparticles synthesized from Fe^0 precursor with various molar ratios. The molar ratios of iron and gold are 1:1, 1:2, and 1:3, indicated by circle, cross, and triangle, respectively.

dominant absorption peaks. The nanoparticles that are obtained from Fe^0 precursor shows the first absorption peak at 395 nm and the second peak at 650 nm. The initial molar ratio of the iron to gold precursor used in this case is 1:2. On the other hand, nanoparticles obtained from Fe^{2+} precursor shows the peaks at approximately 395 and 662 nm, which are shifted relative to the surface plasmon peak of the gold nanoparticles. Gold nanoparticles were prepared under identical conditions to that of alloy nanoparticles. No gold absorption peak has been observed in the plasmon peak of alloy Fe−Au nanoparticles prepared from both Fe^{2+} and Fe^0 precursor. In the case of gold nanoparticles, there is an absence of first peak at shorter wavelength region and only the characteristics peak of gold nanoparticles at 534 nm is observed. The shifted absorption peaks of the Fe−Au alloy nanoparticles relative to the gold nanoparticles could be the result of change in the electron density or the result of the sharp edges of icosahedral structure. A shift in the position of a plasmon peak due to sharp edges has been reported previously in the case of silver nanoparticles with triangular geometry.[18] The concept of hybridization of plasmon bands[19,20] and cavity resonance obviously does not apply because the nanoparticles are not core−shell structures. Another plausible explanation based on literature for the shift is the perturbation of electron cloud oscillation due to surface gold atoms. Specifically, a thin gold layer on the alloy nanoparticles could increase the dielectric constant of the immediate proximity of the particle, plus the plasmon oscillation of a thin gold layer could couple with plasmon oscillation of the alloy nanoparticles and the gold may also transfer electrons to the alloy nanoparticles, resulting in a shift of the plasmon peak.[4,8,14,21] This explanation seems to correlate reasonably well with the experiment. The absorption peak is slightly tunable depending on the amount of iron

incorporated into gold. In the case of gold-coated nanoparticles, there is usually a red shift in the surface plasmon peak position with the decrease in shell thickness and a blue shift with the increase in shell thickness.[8,11,14,22] Figure 3 shows a trend similar to that of core−shell nanoparticles, but less pronounced (20 and 12 nm). There is a blue shift in the 662 nm peak position with increasing amount of gold. When the Fe−Au molar ratio is 1:1, the plasmon peak position is located at 662 nm. On the other hand, when Fe−Au molar ratio is changed to 1:2, the plasmon peak position is blue-shifted to 650 and 642 nm for a 1:3 initial molar ratio of iron to gold precursor. For the first peak, the trend is identical and blue-shifted from 397 nm for a 1:1 initial molar ratio of iron to gold and 385 nm for a 1:3 initial molar ratio of iron to gold precursor. For comparison, the spectrum of water-soluble gold nanoparticles prepared in the absence of iron is also presented in Figure 3. The plasmon peak position of gold nanoparticles is centered at 534 nm. If the amount of gold during the synthesis of Fe−Au alloy nanoparticles is further increased, the gold plasmon peak appears at approximately 506 nm along with the alloy nanoparticle peaks. The nucleation of the gold nanoparticle occurs at about 1:10 initial molar ratios of Fe−Au, which agrees well with the molar composition of the alloy nanoparticles. This observation holds an important clue as to how these nanoparticles are formed. From this, it can be concluded that no heterogeneous nucleation takes place, but gold seems to nucleate along with iron to form the alloy nanoparticles. The lack of heterogeneous nucleation suggests that the alloy particles are thermodynamically more stable than separate gold nanoparticles. No similar statements can be made in comparison with iron nanoparticles because the iron nanoparticle have no distinct plasmon absorption in the visible spectrum.

Curve I in Figure 4a shows the XRD patterns of pure gold nanoparticles and curve II and III represent the Fe−Au alloy nanoparticles which are obtained from Fe^0 and Fe^{2+} with 1:1 initial molar ratio of precursor's molecules. The XRD pattern of the alloy nanoparticles obtained from the Fe^0

(18) Mock, J. J.; Barbic, M.; Smith, D. R.; Schultz, D. A.; Schultz, S. *J. Chem. Phys.* **2002**, *116* (15), 6755–6759.
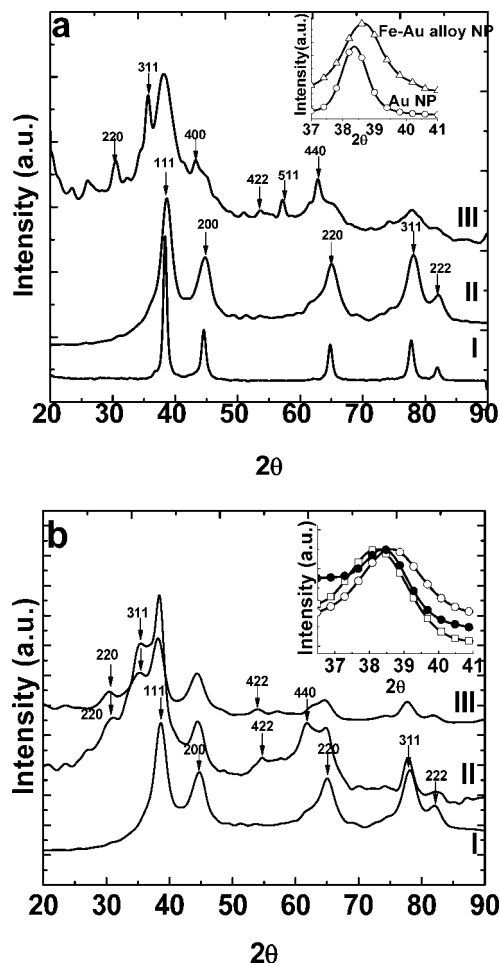(19) Gangopadhyay, P.; Gallet, S.; Franz, E.; Persoons, A.; Verbiest, T. *IEEE Trans. Magn.* **2005**, *41* (10), 4194–4196.
(20) Prodan, E.; Radloff, C.; Halas, N. J.; Nordlander, P. *Science* **2003**, *302* (5644), 419–422.
(21) Lin, J.; Zhou, W. L.; Kumbhar, A.; Wiemann, J.; Fang, J. Y.; Carpenter, E. E.; O'Connor, C. J. *J. Solid State Chem.* **2001**, *159* (1), 26–31.

(22) Wilcoxon, J. P.; Abrams, B. L. *Chem. Soc. Rev.* **2006**, *35* (11), 1162–1194.

Figure 4. (a) XRD patterns of pure gold nanoparticles prepared under identical conditions to that of alloy nanoparticles (curve I) and iron−gold alloy nanoparticles obtained from Fe^0 (curve II) and Fe^{2+} (curve III) precursors. Inset shows the shift of the (111) atomic reflection plane of iron−gold alloy nanoparticles from Fe^0 precursor (open triangle) relative to gold nanoparticles (open circle). (b) (I) is the powder XRD of Fe−Au alloy prepared form Fe^0 precursor and stored in airtight vessel for six months. (II) is the powder XRD of partially oxidized particles stored in water for several days. (III) is the powder XRD of the same particles annealed to 500 °C in air immediately after synthesis. Inset shows the shift in 2θ angle from (111) atomic reflection plane of Fe−Au alloy of the freshly prepared sample (open circle), oxidized (closed circle), and annealed sample at 500 °C (open square).

precursor (curve II) reveals that the samples are crystalline. There is broadening due to smaller particle size and considerable change in 2θ angle compared to pure gold nanoparticles prepared under identical conditions. The shifting of each peak position to higher 2θ values in the alloy sample obtained from Fe^0 indicates softening of the lattice constant and this is due to incorporation of iron into the gold surface. Figure 4a inset shows the change in 2θ angle of 111 atomic reflections of alloy nanoparticles from the Fe^0 precursor that are taken form (curve II) and pure gold nanoparticles (curve I). The 2θ angles at 38.67, 44.81, 65.32, 78.05, and 82.54° in curves II and I of Figure 4a,b correspond to (111), (200), (220), (311), and (222) fcc atomic reflections planes of alloy nanoparticles.[7,8,10] The degree of crystallinity and homogeneity of the sample is best displayed by the alloy nanoparticles obtained from the Fe^0 precursor. The XRD data shows that there is no phase segregation of the elements in

the alloy nanoparticles from Fe^0 precursor. The XRD pattern of the alloy particles obtained from the Fe^{2+} precursor is also (curve III) displayed in Figure 4.The features of the alloy nanoparticle from Fe^{2+} precursor indicate poor crystallinity and inhomogeneity of sample. Specifically, Figure 4a (curve III) shows the peaks of gold and iron alloy and the various reflections of iron oxide (Fe_3O_4) nanoparticles. The XRD peaks at 30.2, 35.5,43.2, 53.2, 57.2, and 62.8° 2θ correspond to (220), (311), (400), (422), (511), and (440) lattice planes for Fe_3O_4 nanoparticles.[8,22,23] This is different from the work of Glavee et al. in which they reported the formation of mixed oxides of iron, iron, and iron boride nanoparticles upon $NaBH_4$ reduction of Fe^{2+} in aqueous solution.[24] A plausible explanation of this present experimental observation is that some of the iron atoms on the surface of alloy nanoparticles are oxidized while using Fe^{2+} precursor. In the Fe^{2+} sample, the (220), (311) and (222) atomic reflection planes for the Fe−Au alloy nanoparticles are small. Synthesis of alloy nanoparticles from the Fe^{2+} precursor results in a mixture of iron oxide (Fe_3O_4) and gold. From these results, one can conclude that Fe^0 precursor is better source to obtain alloy nanoparticles under the experimental conditions used in this study.

The crystallite size of nanoparticles is determined by using the Debye−Scherrer equation: $L = (0.88\lambda)/(\beta\cos\theta)$, where λ is the X-ray wavelength in nm, β is the intrinsic peak width in radians (2θ), the β value is calculated by Gaussian fitting of the most intense atomic reflection (111) peak of Fe−Au alloy nanoparticles, θ is the Bragg angle, and 0.88 is the Debye−Scherrer constant.[10] The crystallite size of Fe−Au alloy nanoparticles prepared from Fe^{2+} precursor calculated from the Fe−Au (111) atomic reflection plane is 6 ± 1.0 nm and the crystallite size of the nanoparticles obtained from Fe^0 precursors is 4.9 ± 1.0 nm. These values are slightly higher than the TEM data (4.9 ± 1.0 and 3.8 ± 1.0 nm), but consistent with the HRTEM images.

Table 2 shows the 2θ angles of Au and Fe−Au alloy nanoparticles. The data in Table 2 indicate that the 2θ angles of Fe−Au alloy nanoparticles of different planes are higher than the corresponding 2θ angles of pure gold. The changes in 2θ angles indicate the reduction of the lattice constant due to alloying gold with iron.[13] The reason of reduction lattice constant is that the atomic radius of iron (126 pm) is smaller than pure gold (144 pm); therefore, the incorporation of iron into gold reduces the lattice constant. An important question here is why the structure is not collapsed after the incorporation of iron. A possible explanation is that the bulk strain of the alloyed particles would become lower by mixing lower atomic radius iron, even if the alloyed nanoparticles grow larger than the critical size of gold nanoparticles.

The Fe−Au sample, which is obtained from the Fe^{2+} precursor, is susceptible to oxidation and mostly it remains in the mixture of iron oxide and gold as examined by XRD analysis. Therefore, the lattice constant and composition is calculated on the basis of the alloy sample prepared form Fe^0 precursor. The average lattice constants of pure gold and

(23) Huber, D. L. *Small* **2005**, *1* (5), 482–501.
(24) Glavee, G. N.; Klabunde, K. J.; Sorensen, C. M.; Hadjipanayis, G. C. *Inorg. Chem.* **1995**, *34* (1), 28–35.

Table 2. Lattice Constants of Fe−Au Alloy and Pure Gold Nanoparticles Obtained from (111), (200), (220), (311), and (222) Atomic Reflections

	pure Au nanoparticles					Fe−Au alloy nanoparticles from Fe^0			
2θ	lattice spacing d (Å)	lattice planes	lattice constant (Å)	average lattice constant (Å)	2θ	lattice spacing d (Å)	lattice planes	lattice constant (Å)	average lattice constant (Å)
38.387	2.3448	111	4.0614		38.679	2.3278	111	4.0319	
44.627	2.0304	200	4.0608		44.817	2.0222	200	4.0445	
64.837	1.4379	220	4.0672	4.0675 ± 0.0375	65.327	1.4283	220	4.0400	4.0449 ± 0.0375
77.791	1.2277	311	4.0719		78.050	1.22431	311	4.0585	
81.861	1.1766	222	4.0761		82.545	1.1686	222	4.0483	

Fe−Au alloy nanoparticles are 4.0675 ± 0.0375 and 4.0449 ± 0.0375 Å, respectively. The reported literature value of lattice constant of pure gold nanoparticles is 4.0782 Å[13] and that of Fe−Au alloy nanoparticles are 4.0550,[13] 4.0312 ± 0.0507,[15] 4.0358 and 3.995 Å.[25,26] Therefore, the lattice constants observed herein are within 0.2−0.3% of experimental error. The reported value of the corresponding lattice constant of fcc bulk iron is 3.590 Å. Obviously, the magnitude of lattice constant of the Fe−Au alloy nanoparticles is between pure gold and pure iron nanoparticles. The substitution incorporation of impurity element allows the application of Vegard's law to estimate the relative portion of the constituents of an alloy sample. According to Vegard's law, there is a linear relationship between the impurity concentration and the lattice constant. The lattice constant of alloy as a function of iron composition x can be approximated using the following formula[27]
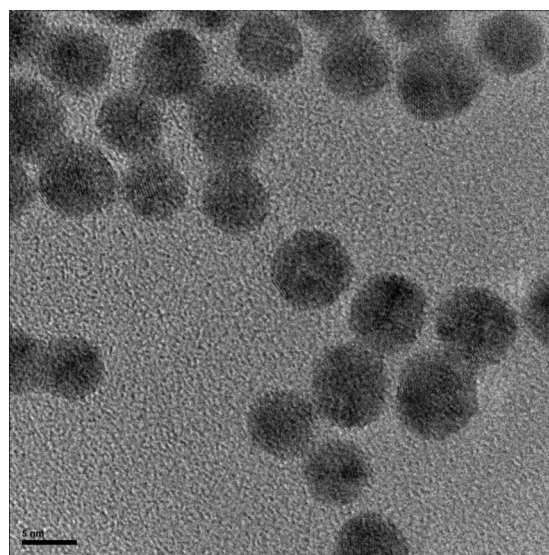
$$a_{\text{Fe−Au}} = (1 - x)a_{\text{Au}} + xa_{\text{Fe}} \qquad (1)$$

where $a_{\text{Fe−Au}}$ is the lattice constant of the alloy nanoparticles prepared from Fe^0 precursor and a_{Au} and a_{Fe} are the lattice constant of gold and iron, respectively. While using the experimental and calculated lattice constant for pure gold and Fe−Au alloy in eq 1, the molar fraction of iron in the alloyed nanoparticles is found to be 4.7 ± 1.5%. When the lattice parameters of the bulk Fe−Au alloys (15.7 and 20% iron content)[15,25,26] are used instead of the pure gold and iron, the composition is 14.8 ± 4.7% iron.[28] This result agrees well with the composition that is obtained from energy-dispersive X-ray analysis and compositions of the previously synthesized Fe−Au alloy nanoparticles (6.50,[13] 11,[12] and 17%[15] iron).

The washed, dry sample can be stored for several months. Curve I in Figure 4b shows the XRD pattern of the Fe−Au alloy obtain from Fe^0 precursor stored in airtight vessel for 6 months. The XRD pattern shows that there is not a phase segregation of alloy nanoparticles. The XRD pattern is similar to curve I in Figure 4a, which is obtained immediately after synthesis. When the sample is stored dissolved in water for several days, the distinct green color of the sample disappears and brown precipitates form. The XRD pattern of the precipitate is shown in Figure 4b (II). The pattern still shows the position of alloy peaks, but broader with additional peaks of iron oxides (Fe$_3$O$_4$) because of the oxidation of iron. The additional peaks are due to iron oxide

(Fe$_3$O$_4$) and correspond to (220), (311), (422), and (440) atomic reflections. This result shows that there is a change in morphology and size of alloy nanoparticles because of oxidation of iron and the phase segregation of gold. When the sample is annealed at 500 °C in air (Figure 4b (III)), sharp peaks due to aggregation and crystal growth are observed. Comparison of the (111) reflection of the annealed Fe−Au alloy nanoparticles and the oxidized samples are shown in the inset of Figure 4b. The annealed sample peak position is shifted completely to the peak position of gold whereas the oxidized sample is not completely shifted to the original peak position of gold (38.2°). The results imply that there is complete phase segregation in case of the annealed sample while with the oxidized sample only partial phase segregation. The major driving force for the segregation of alloy nanoparticles is to minimize its surface energy. At room temperature, the surface free energies for thin films of iron and gold are 2.9 and 1.9 J m^{-2}, respectively,[29] which suggests that in the absence of oxygen the gold is favored at the surface of the particles.

Figure 5 represents the HRTEM images of Fe−Au alloy nanoparticles from the Fe^0 precursor with initial molar ratio of precursor's molecules 1:1. The figure clearly shows not only that the incorporation of gold into iron changes the structure from bcc to fcc but it also indicates the presence of stable icosahedral structures. Saha et. al[12] have also shown the presence of icosahedral structures using a very high temperature heating (1600 K) synthesis method. HRTEM results from this work show very similar structure and

(25) Turkevich, J. G. G.; Stevenson, P. C. *J. Colloid Sci.* **1954**, *8*, S26–35.
(26) Kubaschewski; O, E., H. Z., *Elektrochem. Angew. Phys. Chem.* **1994**, *50*, 138–144.
(27) Zhou, D.; Usher, B. F. *J. Phys. D: Appl. Phys.* **2001**, *34* (10), 1461–1465.
(28) Crangle, J.; Scott, W. R. *J. Appl. Phys.* **1965**, *36*, 921.
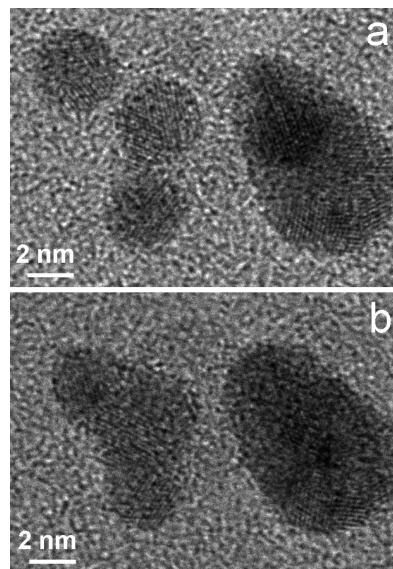
Figure 5. HRTEM image of Fe−Au alloy nanoparticles obtained from Fe^0 precursor with a 1:1 initial molar ratio of precursor molecules. The image shows that the majority of the particles possess icosahedral structures.
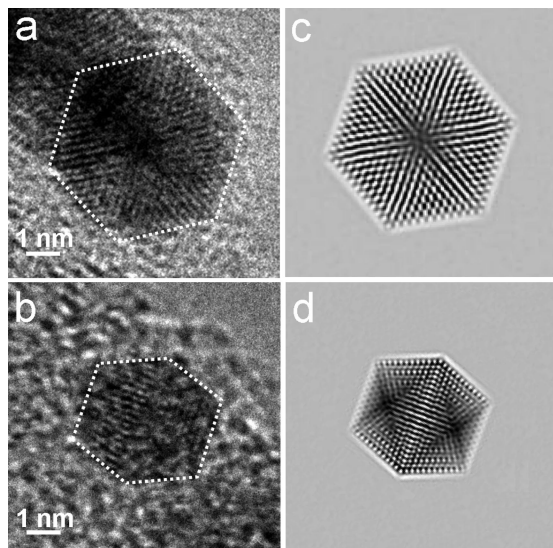
Figure 6. (a,b) HRTEM images of two Fe−Au alloy nanoparticles formed in the icosahedral structure from Fe^0. These particles are oriented: (a) almost along the 3-fold axis and (b) close to the 2-fold axis, respectively. (c, d) Corresponding theoretical HRTEM images from Saha et al.[12] calculated for an icosahedral model structure. Reproduced with permission from ref 12. Copyright 1999, EDP Sciences.

morphology. Images a and b in Figure 6 highlighted the icosahedral crystal structure of alloy nanoparticles with nearly 3- and 2-fold axis of symmetry. Images c and d in Figure 6 are the simulated images of the same particles representing clearly the 3- and 2-fold axis of symmetry in these structure.

Koga et al.[30] also showed the presence of icosahedral structure in the case of gold nanoparticles. During a HRTEM study conducted in conjunction with extensive tilting of gold nanoparticles they have found the presence of icosahedral structure either for 3 nm size or above 8 nm size and not in the 4−6 nm size range. As shown in Figure 5, the majority of the particles possess icosahedral structures in the 3−6 nm size range. Interestingly, there is no observance of decahedral structure like gold nanoparticles. This indirect piece of evidence further supports that there is alloying of iron in gold and change in crystal structure to the icosahedral form. Most of the nanoparticles reveal the Fe−Au alloy (111) lattice fringes with the lattice spacing of ∼0.22 nm. For some of the nanoparticles, the Fe−Au alloy (200) lattice fringes with the spacing of ∼0.20 nm can also be seen, however as opposed to the XRD, the HRTEM technique do not provide sufficient *d*-spacing measurement precision to differentiate between pure gold and Fe−Au alloy.

The nanoparticles also demonstrate some interesting aggregation under the electron beam during HRTEM studies. Figure 7 shows two snapshots of the same area on the sample taken 2 min apart. The images indicate that illuminating the particles with highly converged electron beam, appropriate for HRTEM imaging, initiates the particle fusion by providing sufficient kinetic energy for the particle to migrate toward each other. The energy from the electron beam is not enough though to recrystallize the fused nanoparticles on the time scale of the observation.

(29) Pastor, C. J.; Limones, C.; Hinarejos, J. J.; Garcia, J. M.; Miranda, R.; GomezGoni, J.; Ortega, J. E.; Abruna, H. D. *Surf. Sci.* **1996**, *364* (1), L505−L510.
(30) Koga, K.; Sugawara, K. *Surf. Sci.* **2003**, *529* (1−2), 23−35.

Figure 7. (a, b) HRTEM images of Fe−Au alloy nanoparticles from Fe^0 precursor before and after 2 min exposure of the specimen with a condensed electron beam. Notice the electron-beam-induced fusion of the three nanoparticles located on the left.
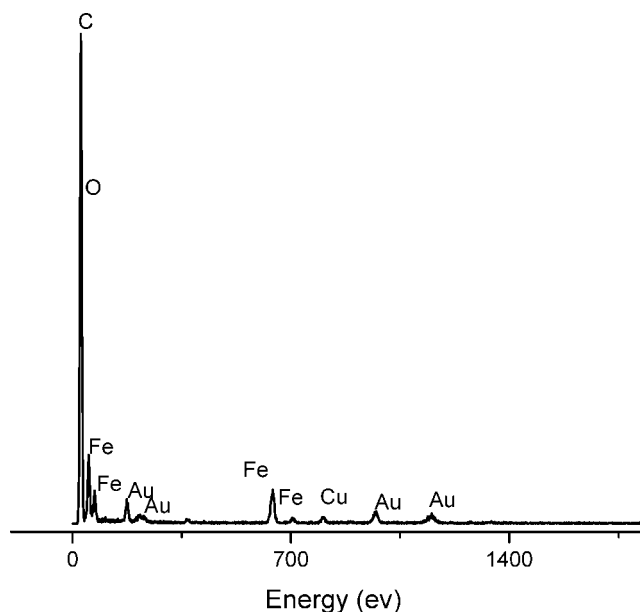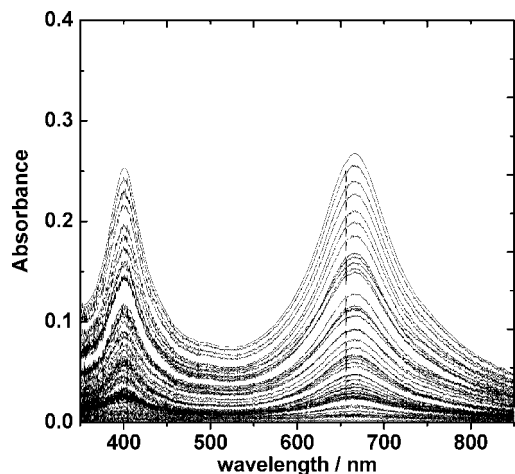

Figure 8. Energy-dispersive X-ray spectroscopy (EDS) analysis of Fe−Au alloy from Fe^0 precursor.

The composition of alloy nanoparticles obtained from Fe^0 is analyzed by energy-dispersive X-ray spectroscopy (EDS). The initial molar ratio of precursor molecules in the sample is 1:1. An electron beam, converged to a diameter of few tens of nanometer, is used to illuminate a cluster of the Fe−Au nanoparticles and an EDS signal is collected. A typical EDS spectrum obtained from such measurements is shown in Figure 8. The appearance of various prominent peaks of gold and iron confirm the presence of these elements. The presence of oxygen indicates that some of the iron particles are oxidized to iron oxide (and the surface ligands contain oxygen as well). The measured iron-to-gold atomic ratio of 20: 80% is slightly higher than the one obtained from the Vegard's law analysis of the XRD data $(14.8 \pm 4.7\%)$ but this is only because there is additional

Figure 9. The UV−visible absorption spectra (in water) of Fe−Au alloy nanoparticles from the Fe^{2+} precursor showing the oxidation trend.

iron present in the form iron oxide particles. Therefore, the EDS data are consistent with the data obtained from the Vegard's Law-based estimation.

The particles synthesized by using the two different precursors have different stability. When they are kept dry, both particles can be stored indefinitely (a few months has been tested). The Fe^{2+} synthesized particles are less stable. Once the nanoparticles from Fe^{2+} are dissolved in water, they lose their distinct green color and transform into a rust-colored precipitate in approximately 30 min. The nanoparticles prepared from Fe^{0} precursor remains stable for a significantly longer period. The lifetime of the particles can be extended if they are kept in the dark. Figure 9a represents the UV−visible spectra of gold iron alloy nanoparticles of Fe^{2+} precursor. The spectra are recorded in equal time intervals for 30 min. Figure 9 shows that the absorption peaks associated with the particles completely disappear after 30 min. The disappearance of the plasmon peak may be due to (1) the loss of ligands from the alloy nanoparticles and (2) any unreacted sulfate ions further facilitating the oxidation of iron via redox eqilibria. The width of the peaks (not shown) do not change over time, but rather only decrease in intensity, which suggests that once a particle becomes unstable the oxidation is fairly fast on the time scale of the observation.

Conclusions

In summary, a facile synthesis of water-soluble Fe−Au alloy nanoparticles with relative low iron content is demonstrated. The results show that the particle synthesized from iron pentacarbonyl shows higher stability. The absorption of the nanoparticles shows interesting double peak plasma resonance.